SSC21-WKV-03

Performance Comparison of Particle Filter in Small Satellite Attitude Estimation

Asma Mohammad Nusrat Aman, Nafizah G. Khan, Gnanam Gnanagurunathan
Department of Electrical & Electronic Engineering, University of Nottingham Malaysia, Semenyih 43500, Malaysia
asma.nusrat.17@gmail.com

ABSTRACT

The drive towards miniaturization, coupled with the latest advances in onboard processing, has given rise to small satellite missions' ability to use more complex attitude estimation algorithms to fit their progressive mission requirements. Earth observation missions typically require higher satellite attitude pointing accuracies to precisely control the satellite orientation. Hence, to provide greater confidence in the attitude estimation accuracies, new advanced algorithms are continuously being developed. Satellite attitude estimation must be performed autonomously in real-time whilst optimizing computational resources such as time and memory. Small satellite missions with higher complexities tend to demand more sophisticated requirements, which push the limits of classical attitude estimation methods. The Particle Filter is an advanced Bayesian estimation technique that has shown significant improvements in satellite attitude estimation. This work describes the Particle Filter and its implementation to the attitude and angular rate estimation for a 3U CubeSat in Low Earth Orbit, whilst comparing attitude estimation performance in two different settings: with three-axis magnetometer measurements; and with combined measurements from a three-axis magnetometer and sun sensors. This work further reports that for attitude determination in small satellites, the Particle Filter is a more accurate attitude estimator than the widely used Extended Kalman Filter. The Particle Filter yields attitude estimation accuracy of ±0.01°, while the Extended Kalman Filter attitude estimation accuracy is ±1°. Moreover, the results indicate that the use of an additional sensor improves the attitude estimation accuracy of the Particle Filter by 17%. It is essential to consider different sensor combinations as it helps select the most suitable sensor suite and attitude estimator for an individual small satellite mission.

INTRODUCTION

Cube Satellites (CubeSats) are standardized form of small satellites with strict dimensions and mass restrictions, which have recently become widely commercialized and prevalent. A 1–Unit (1U) CubeSat has a standard size of $10 \times 10 \times 10\ cm$ and mass of $1.33\ kg$. Several 1U's stacked together make up 2U, 3U, 6U CubeSats. Such CubeSats are quick to manufacture and rely on low-cost and low-weight COTS hardware. They have become widely used for applications such as Earth imaging, that require CubeSats to be three-axis stabilized to point cameras or payload in desired directions. Hence, the satellite must determine its current pointing direction (orientation) accurately first, performed by the satellite's attitude determination and control system (ADCS). The attitude of a satellite is defined as its orientation in space with reference to an inertial frame.

Attitude determination is performed by sampling data from attitude sensors and processing that data to estimate the attitude via attitude estimation methods. A few simple attitude determination algorithms include TRIAD, Q-Method, Least Squares, that focus on solving Wahba's problem and do not consider the attitude dynamics model and measurement uncertainties. Other methods that consider statistics of process and measurement noise are the Kalman filter and its variants, Particle filters, H-infinity filters, etc. These attitude estimation methods rely on the statistical measures of system noise and use the attitude dynamics and kinematics models to propagate the state to be estimated. Types of attitude sensors used onboard CubeSats in Low Earth Orbit (LEO) include magnetometer, star tracker, sun sensor, and gyroscope. Magnetometers and sun sensors are commonly used due to their simplicity, accessibility, and low-cost. The use of one sensor may be enough, for example, in the case of a three-axis magnetometer for CubeSat in LEO. However, using a combination of measurements adds benefits like robustness in operational performance, redundancy in case of data loss or sensor failure, and

increased confidence in the inferred results, leading to reduced uncertainty in estimations [1]. The most accurate sensor suite for satellite attitude estimation is the star tracker; but it is heavy, has a very high computational burden, and is expensive. Magnetometers are the best option for LEO CubeSats, as they are lighter, cheaper, and the magnetic field is always available to measure and compared with the most updated Earth Magnetic Field model. Combining sun sensor measurements with three-axis magnetometer measurements is expected to improve performance while maintaining low cost and low weight requirements of CubeSats. This work shows that it adds very little to increase computational burden as well. Moreover, gyroless attitude estimation is desired in small satellites, as gyros are prone to degradation and failure, and gyro drift usually must be estimated and corrected, which adds further computational burden [2].

In the design of ADCS, the focus is on the rotational dynamics of the satellite, consisting of attitude dynamics and kinematics – which are generally nonlinear in nature – meaning they cannot be written as simple linear combinations of the unknown variables (satellite attitude and angular rate). In addition, the process and measurement noise in the satellite attitude system, which may emerge from disturbance torques acting on satellite body or attitude sensor noise respectively, are usually assumed to have Gaussian distributions, but they may not be Gaussian in nature. That is, random noise statistical properties may not have a normal distribution. The most widely used nonlinear satellite attitude estimator is the Extended Kalman Filter (EKF). The EKF linearizes the nonlinear dynamics to the current state, using Taylor series to obtain Jacobians to help propagate the state, and applies an assumption of Gaussian noise characteristics. The linearization and Gaussian assumption affect accuracy as it is an imprecise approximation of the attitude dynamics model and does not reflect reality. The Unscented Kalman Filter (UKF) maintains the nonlinearity of the equations but upholds the Gaussian assumptions. If the statistical distribution of the processes driving the dynamic model is non-Gaussian distributions, the estimates will not be optimal [3]. The Particle filter (PF), on the other hand, works well with nonlinearity in attitude dynamics, as well as non-Gaussian assumptions.

The PF is a nonlinear estimation algorithm based on a recursive Bayesian approach that approximates nonlinear functions using a set of random particles without restrictions to specific noise distributions [3]. The benefits of PF are that it does not need to linearize the nonlinear attitude dynamics, and it makes no assumptions on the noise distributions. This is highly favorable in a CubeSat in a LEO environment as the process and measurement noise sources may be unpredictable and their actual statistical behavior unknown. The basic principle of the PF algorithm is briefly described here, with more details given in the next section. The following equations define a general discrete-time nonlinear system:

$$x_{k+1} = f(x_k) + w_k \tag{1}$$

$$y_k = h(x_k) + v_k \tag{2}$$

where Equations (1) and (2) are called the state and measurement equations respectively; $x_k \in R^n$ is the state vector with dimension n, $y_k \in R^m$ is the measurement vector with dimension m, f and h are the nonlinear functions of system and measurement respectively, w_k and v_k represent the stochastic process and measurement noise respectively, and k is the discrete time step.

The PF represents probability density functions (PDFs) by using a random set of N particles $\{x_k^i\}_{i=1}^N$ of the states, where i is particle index, along with their associated weights $\{W_k^i\}_{i=1}^N$. The recursive process is implemented by prediction-update at each time step. The state equation (Equation 1) characterizes the state transition probability function of the system given as $p(x_{k+1}^i|x_k^i)$, which describes the prediction step that propagates the current state, to predict the future state for the next time step. In the prediction step, each particle is advanced one-step ahead through Equation 1. The measurement equation (Equation 2) characterizes the likelihood probability function given as $p(y_k|x_{k+1}^i)$, which describes the update step, that uses the measurements to evaluate the posterior by weighting particles proportional to their likelihood. The weights

assigned to each particle are calculated using Bayes' rule and given as

$$W_{k+1} = \frac{W_k \; p(y_k|x^i_{k+1}) p(x^i_{k+1}|x^i_k)}{q(x^i_{k+1}|x^i_{0:k}, y_{1:k})} \quad (3)$$

where $q(x^i_{k+1}|x^i_{0:k}, y_{1:k})$ is the importance density function. Particle weights are then normalized, as their sum should equal 1, since they represent the probability that a state is predicted accurately, according to the measurement at the time.

$$W^i_k = \frac{W^i_k}{\sum_{i=1}^{N} W^i_k} \quad (4)$$

The importance weights are computed based on the measurements from the sensors. The particles which are closer to the measured attitude (i.e. more likely to be accurate) are given higher weights, while those that are further from the measured values are assigned lower weights and eventually discarded during resampling. The posterior PDF is then recursively approximated through Monte Carlo simulations by using the weights

$$p(x_{k+1}|y_{1:k}) \approx \sum_{i=1}^{N} W^i_{k+1} \delta(x_{k+1} - x^i_{k+1}) \quad (5)$$

where $\delta(.)$ is the Dirac delta function, which indicates the distribution that models the density of a particle. With a large number of particles N, the PDF representation gives an accurate estimate of the state. Finally, a resampling step eliminates particles with lower importance weights and multiplies particles with higher importance weights.

The use of vector measurements for attitude estimation in small satellites has been vastly investigated throughout the literature. Also, comparisons with different sensor combinations have been done to test the performance of attitude estimators. The EKF has been applied to estimate satellite attitude using three-axis magnetometer and sun sensors, with an attitude estimation accuracy of 1° [4], [5]. Furthermore, different sensor combinations were investigated for the EKF, and varying estimation accuracies were reported for each combination [6]. The PF has been proposed for satellite attitude estimation and has shown improved performance compared with traditional approaches such as the EKF and UKF. Modifications to the standard PF formulation have also been proposed to further improve performance and/or reduce computational cost. PF variants that have been proposed for satellite attitude estimation include the marginalized PF [7], an adaptive PF [3] and Rao-Blackwellized PF [8]. Methods have also differed in their choice of attitude representation and sensor(s) selection. A PF with attitude represented by Modified Rodrigues Parameters (MRPs) considered gyros and star tracker sensor combinations [2]. A PF with attitude represented by Generalized Rodrigues Parameters (GRPs) considered magnetometer and gyro measurements, while the performance was compared to that of UKF [9]. An Unscented PF was proposed for satellite attitude estimation using star tracker, with attitude error of ±0.0009° reported [10].

This paper focuses on two different sensor configurations for the PF attitude estimator, whereby the performance of the two cases is compared. The simulation of attitude dynamics of a 3U CubeSat in sun-synchronous LEO is done via Matlab. The PF algorithm for attitude and angular rate estimation is implemented using i) simulated three-axis magnetometer measurements only, and ii) a combination of three-axis magnetometer and sun sensors measurements. The aim is to determine whether the addition of a second sensor could improve attitude estimation results and prove the superior performance of the PF algorithm compared to the widely used EKF. The satellite attitude and measurement models are described in the next Section. Next, the PF algorithm is briefly described. To gauge the attitude estimation performance of PF, the EKF is also implemented. Next, the simulation results and analysis are presented. Finally, the main conclusions are reported.

SATELLITE ATTITUDE ESTIMATION USING PARTICLE FILTER

Satellite Attitude Model

The satellite attitude motion is described by kinematic and dynamic equations. The nonlinear dynamic model of a rigid body satellite is given as the differential equation relating the rate of change of satellite angular rate to the torques acting on the satellite and the Inertia components of the satellite, realized from the Euler equation of motion for rigid body dynamics, given by

$$\dot{\omega} = \begin{bmatrix} \dot{\omega}_x \\ \dot{\omega}_y \\ \dot{\omega}_z \end{bmatrix} = \begin{bmatrix} -\left(\frac{I_z - I_y}{I_x}\right)\omega_y\omega_z + \frac{\tau_x}{I_x} \\ -\left(\frac{I_x - I_z}{I_y}\right)\omega_x\omega_z + \frac{\tau_y}{I_y} \\ -\left(\frac{I_y - I_x}{I_z}\right)\omega_x\omega_y + \frac{\tau_z}{I_z} \end{bmatrix} \quad (6)$$

where ω is the 3×1 satellite angular rate vector with respect to an inertial frame, about the x-axis (ω_x), y-axis (ω_y), and the z-axis (ω_z), given in degrees per second. $I_{x,y,z}$ represents the respective moments of inertia in all three (x,y,z) axes, and $\tau_{x,y,z}$ signifies the gravity-gradient disturbance torque elements acting on the CubeSat body in LEO.

While there are several representations for satellite attitude, quaternion rotations are used to avoid the singularity issue that arises in Euler angles representation. The quaternion $q = [q_1 \quad q_2 \quad q_3 \quad q_4]^T$ is a four-dimensional vector used to represent the satellite attitude. The satellite attitude kinematics equation describes how the quaternion attitude changes under the influence of the satellite angular rate. The quaternion differential kinematic equation is given by

$$\dot{q} = \begin{bmatrix} \dot{q}_1 \\ \dot{q}_2 \\ \dot{q}_3 \\ \dot{q}_4 \end{bmatrix} = \frac{1}{2}\begin{bmatrix} 0 & \omega_z & -\omega_y & \omega_x \\ -\omega_z & 0 & \omega_x & \omega_y \\ \omega_y & -\omega_x & 0 & \omega_z \\ -\omega_x & -\omega_y & -\omega_z & 0 \end{bmatrix}\begin{bmatrix} q_1 \\ q_2 \\ q_3 \\ q_4 \end{bmatrix} \quad (7)$$

The combined state equation of the satellite attitude model is given in terms of the satellite quaternion attitude and angular rate in state space formulation following notations in Equation 1 as follows

$$\dot{x}_k = \begin{bmatrix} \dot{q} \\ \dot{\omega} \end{bmatrix} = \begin{bmatrix} \frac{1}{2}\Omega(\omega)q \\ I^{-1}(\tau - \omega \times I\omega) \end{bmatrix} + w_k \quad (8)$$

where w_k is the process noise, modelled as zero-mean Gaussian white noise and $\Omega(\omega)$ is the anti-symmetric matrix of ω, given as

$$\Omega(\omega) = \begin{bmatrix} 0 & \omega_z & -\omega_y & \omega_x \\ -\omega_z & 0 & \omega_x & \omega_y \\ \omega_y & -\omega_x & 0 & \omega_z \\ -\omega_x & -\omega_y & -\omega_z & 0 \end{bmatrix} \quad (9)$$

Measurement Models

The measurement model describes how the states are related to the sensor measurements. The difference in the simulations of PFs in this study is in the measurement models used. The measurement equation gives either combined measurement readings (from three-axis magnetometer and sun sensors) for PF-2, or measurement readings from only three-axis magnetometer (for PF-1). Measurements are given in terms of the state, and the added sensor noise with known statistical properties, following Equation 2. The general measurement model is given as

$$y_k = h(x_k) + v_k = A(\bar{q}_k) \cdot r_k + v_k \quad (10)$$

where y_k is the measurement vector, h_k is the nonlinear measurement function, r_k is the relative vector measurement from sensor obtained at time step k in an inertial frame, and v_k is the measurement noise, modelled as zero-mean Gaussian white noise. $A(\bar{q}_k)$ is the rotation that describes the rotation from inertial vector to body vector, given by

$$A(\bar{q}) = (q_4^2 - q_{13}^T q_{13})I_{3\times3} - 2q_4[q_{13}\times] + 2q_{13}q_{13}^T \quad (11)$$

where q_{13} represents the first three elements of the attitude quaternion, q_4 represents the fourth element of the attitude quaternion, and $I_{3\times3}$ is the 3×3 identity matrix.

Magnetometer Model

Magnetometers are vector-based attitude sensors that measure the direction and magnitude of the Earth's magnetic field around the satellite. The three-axis magnetometer (TAM) provides information about the Earth magnetic field for all three axes. The International Geomagnetic Reference Field (IGRF) model simulates the Earth's magnetic field in the Earth-centered-inertial (ECI) frame. The simulated three-axis magnetometer measurement gives the magnetic field in

the satellite body frame by multiplying the rotational matrix $A(\bar{q})$ from Equation 11, with the magnetic field vector in the ECI frame, given by the IGRF model. The magnetometer model is given by

$$\mathbf{B}_{meas} = A(\bar{q})\mathbf{B}_{ECI} + \mathbf{v}_{mag} \quad (12)$$

where $\mathbf{B}_{meas}$ is the output measurement vector of the magnetometer, representing the measured Earth magnetic field in satellite body frame; $\mathbf{B}_{ECI}$ is the Earth magnetic field vector in an inertial frame (analogous to r_k in Equation 10 – given by the IGRF output); and $\mathbf{v}_{mag}$ is the measurement noise associated with TAM, assumed to be zero-mean Gaussian with standard deviation σ_m along each axis.

Sun Sensor Model

The simulated sun sensor measurement is a vector of the sun's relative position with respect to the center of the satellite body frame. It is assumed that six sun sensors are placed on each side of the CubeSat. To simulate the sun sensor output, the motion of the satellite around the Earth (obtained from the orbit propagator model) and motion of Earth around the sun are modelled. The sun sensor model is given by

$$\mathbf{S}_{meas} = A(\bar{q})\mathbf{S}_{ECI} + \mathbf{v}_{sun} \quad (13)$$

where $\mathbf{S}_{meas}$ is the output measurement vector of the sun sensors and represents the normalized measured vector from satellite to sun in body frame, $\mathbf{S}_{ECI}$ is the sun directional vector in an inertial frame, and $\mathbf{v}_{sun}$ is the measurement noise associated with the sun sensor, assumed to be zero-mean Gaussian with standard deviation σ_s along each axis.

Particle Filter for Attitude Estimation

In the satellite attitude estimation formulation, the state to be estimated contains the satellite attitude in quaternion and the satellite angular rates, given as $x = [q \quad \omega]^T = [q_1 \quad q_2 \quad q_3 \quad q_4 \quad \omega_x \quad \omega_y \quad \omega_z]^T$, where x is the 7×1 state vector, q is the 4×1 quaternion attitude, and ω is the 3×1 angular rate vector. The PF algorithm for attitude estimation is described below

1. Initialization:

The PF algorithm is initialized by generating a set of initial N particles $\{x_0^i\}_{i=1}^N$ that represent a-priori distribution of the state from initial distribution $p(x_0)$. Each particle is assigned a weight that is set to $W_0^i = \frac{1}{N}$ for $i = 1,2, \ldots, N$.

2. Prediction:

For $k \geq 1$, the particles $\{x_k^i\}_{i=1}^N$ are propagated by $x_k^i \sim p(x_{k+1}^i | x_k^i)$ to obtain a set of sampled states $\bar{x}_k^i, i = 1, \ldots N$.

3. Update:

Once the measurement y_k is obtained, the weight of the particle is evaluated via Equation 3 and weights are then normalized by Equation 4. The particles are assigned weights equal to the probability of observing the sensor measurements given the particle state $p(y_k | x_{k+1}^i)$. Particle weights are modified whenever measurements are made available. An updated set of posterior particles are obtained $\{\bar{x}_k^i, \widetilde{W}_k^i\}$.

4. Resampling:

A new set of particles is generated $\{x_k^j\}_{j=1}^N$ by resampling N times from $\{x_k^i\}_{i=1}^N$, where $p(x_k^j = x_k^i) = W_k^i$, and set $W_k^j = 1/N$.

5. Estimation:

The mean state vector is estimated according to

$$\hat{x}_k = \sum_{i=1}^{N} W_k^i x_{k,k+1}^i \quad (14)$$

and the algorithm is repeated from Step 2 onwards to estimate the state at the next time step.

The initialization, prediction, estimation, and resampling steps for the two PFs simulated are the same. The difference lies in the update step (Step 3), since the likelihood and importance density are dependent on the measurement models, which result in a different set of updated weights for PF-1 and PF-2. Equation 3 of the PF algorithm indicates that the importance density, which is dependent on the probability of the state given the measurement, is inversely proportional to the likelihood weight. This implies that higher weight is assigned to a state with a 'highly probable' proposal distribution. In PF-2, the proposal distribution is further decreased with the additional sensor measurements via sensor fusion, giving a higher prospect of more accurate states, and hence is expected to have lower values of attitude estimation error.

EKF Algorithm

The EKF linearizes the nonlinear Equations 1 and 2, and they are approximated as follows

$$x_{k+1} = F_k x_k + w_k \quad (15)$$

$$y_k = H_k x_k + v_k \quad (16)$$

where F_k is the linearized state transition matrix, H_k is the measurement matrix, and w_k and v_k are the process and measurement noise respectively. F_k and H_k are derived by taking partial derivatives of the dynamics and measurement equations via Taylor series expansion. The PDFs of noises are Gaussian with zero means, represented by $p(w_k) \sim N(0, Q)$ and $p(v_k) \sim N(0, R)$, where Q is the process noise covariance matrix, and R is the measurement noise covariance matrix. F_k is used to propagate the error covariance matrix P_k. The EKF algorithm consists of time update and measurement update equations. The EKF algorithm for attitude estimation is given as

1. Initialization:

At time $k = 0$, the PDF of the initial state is Gaussian and known $p(x_0)$.

2. Time Update:

The state estimate is propagated using the linearized state transition function F_k

$$\hat{x}_{k+1} = F_k \hat{x}_k \quad (17)$$

The state error covariance matrix is then propagated

$$P_{\bar{k}+1} = F_k P_k F_k^T + Q_k \quad (18)$$

3. Measurement Update:

The Measurement Update equations constitute Kalman gain matrix calculation used as feedback for correcting state estimates.

$$K_k = P_{\bar{k}} H_k^T (H_k P_{\bar{k}} H_k^T + R_k)^{-1} \quad (19)$$

And state estimate and error covariance matrix are updated as follows

$$\hat{x}_k = \hat{x}_{\bar{k}} + K(y_k - H_k \hat{x}_{\bar{k}}) \quad (20)$$

$$P_k^+ = (I - K_k H_k) P_{\bar{k}} \quad (21)$$

Steps 2 and 3 are repeated recursively to give the state estimate for all time steps. Note that the EKF implemented in the simulations takes measurements from both sun sensors and three-axis magnetometer.

SIMULATION RESULTS

Simulations are performed on Matlab to demonstrate the performance of the attitude estimation algorithms. To be able to estimate satellite attitude, the attitude determination system must have access to inputs such as: the satellite position (obtained from SGP4 orbit propagator), the sun position relative to the satellite (calculated from satellite position and Julian date), the Earth's magnetic field model (computed via the IGRF model), and the satellite characteristics (inertia matrix, satellite mass, and satellite dimension). The satellite dynamics and kinematics (Equations 6 and 7) are integrated using Runge-Kutta (RK4) integration. The magnetometer vector measurement is calculated using Equation 12, while the sun sensor vector measurement is given by Equation 13. PF-1 uses only three-axis magnetometer as attitude sensor in the simulations, while PF-2 combines three-axis magnetometer and sun sensor measurements. It is assumed that the simulated

sensors are calibrated against biases, and therefore, only zero-mean Gaussian white noise error is considered, with the standard deviation values for each given in Table 1, along with the relevant simulation parameters.

In both the PFs, $N = 1000$ particles are used.

Table 1: Simulation parameters for attitude estimation.

Simulation Parameter	Value	
Total Simulation Time	5800 $seconds$ ~ 1 orbit	
Orbit	Sun-synchronous LEO, with an altitude of 635 km, and inclination of 97.8°	
Small Satellite Properties	CubeSat Type	3U
	Mass	3.5 kg
	Dimensions	$0.34\ m \times 0.10\ m \times 0.10\ m$
	Inertia matrix	$\begin{bmatrix} 0.0058 & 0 & 0 \\ 0 & 0.0366 & 0 \\ 0 & 0 & 0.0366 \end{bmatrix} kgm^3$
Simulated Three-Axis Magnetometer	Earth Magnetic Field Model Used	IGRF – 13
	Magnetometer Error	$\sigma_m = 300\ nT$
Simulated Sun Sensor	Sun Sensor Error	$\sigma_s = 0.05°$
Initial satellite attitude and angular rate	$\varphi = 10°, \theta = 5°, \psi = -2°$ $\omega_x = 0.05\ °/s, \omega_y = 0.1\ °/s, \omega_z = 0.5\ °/s$	

To evaluate and compare the performances of the two PFs, the attitude and angular estimation errors are considered. Due to lack of physical interpretation, the estimated attitude quaternion is converted to Euler angles (Roll, Pitch and Yaw) to analyze the results. The attitude estimation error is defined as the difference between the true values of attitude vector propagated and the estimated attitude results. Figure 1 shows the attitude errors in terms of the Roll (ϕ), Pitch (θ) and Yaw (ψ), and Figure 2 shows the angular rate errors for PF-1, PF-2, and EKF. As evident from the plots, there is a distinction between attitude and angular estimation errors for both the PFs and these are investigated further. The EKF errors, on the other hand, appear to be much more prominent in comparison. This demonstrates the ineffectiveness of the EKF to estimate the satellite attitude accurately, due to linearization of the nonlinear satellite attitude dynamics.

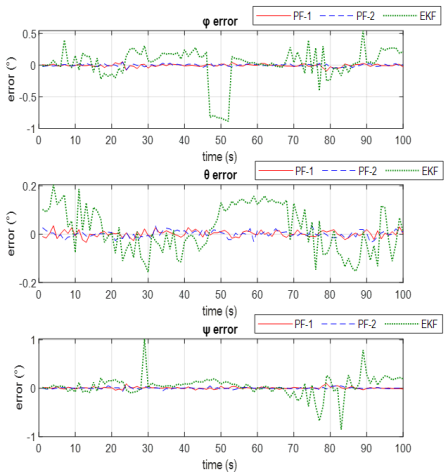

Figure 1: Plots of attitude estimation error.

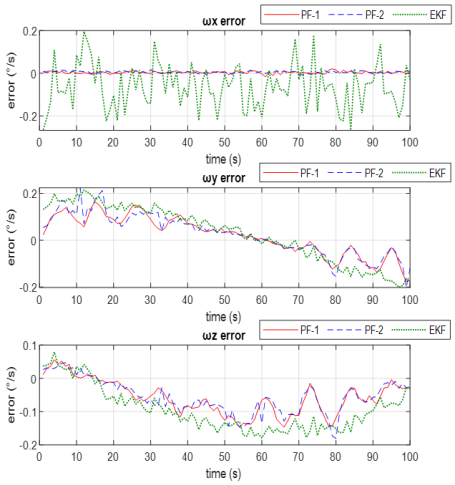

Figure 2: Plots of angular rate estimation error.

A fundamental aspect of estimation methods is their estimation performance, which may be given in terms of the root mean square error (RMSE) and mean absolute error (MAE). The smaller the RMSE value resulting from the filter, the better the filter performance, and the estimator is more accurate. Figure 3 illustrates the comparisons of the norm of attitude RMSEs for PF-1, PF-2, and EKF. The error values decrease before settling to a steady-state error, indicating that the PFs converge quickly and successfully.

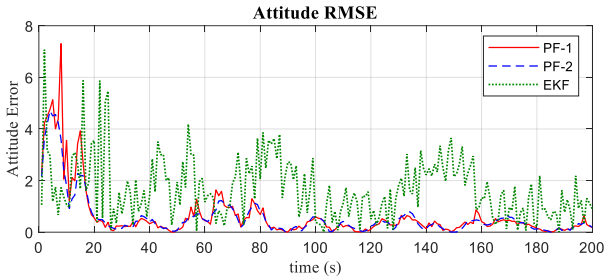

Figure 3: Plots of RMSE of attitude estimates.

Furthermore, the Mean Absolute Error (MAE) between the actual attitude and the estimated attitude is calculated. The MAE represents the average of absolute values of a set of estimation errors. Table 2 compares the results of the steady-state MAE for PF-1, PF-2, and EKF for attitude and angular rate estimation errors.

Table 2: Steady state MAE values for attitude and angular rate estimation errors.

Attitude Estimation Algorithm	Attitude Error (°)			Angular Rate Error (°/s)		
	φ	θ	ψ	ω_x	ω_y	ω_z
PF-1 (MAG-only)	0.0438	0.0103	0.0361	0.0059	0.0678	0.0668
PF-2 (MAG+SUN)	0.0139	0.0101	0.0151	0.0059	0.0683	0.0683
EKF	1.3730	0.6221	1.0530	0.0909	0.6548	0.6446

From Table 2, PF-1 has larger attitude estimation error values than attitude error values in PF-2. Therefore, the estimation accuracy of PF-2 is said to be higher than that of PF-1, which is as expected since the addition of an extra attitude sensor (the sun sensor in PF-2) must provide a higher attitude estimation accuracy. The estimation performance of PF-1 is slightly worse since the reliability of a single sensor configuration degrades estimation performance. In contrast, PF-2 rapidly converges and maintains high estimation accuracy. Comparatively, the EKF shows inferior estimation performance.

Another aspect of attitude estimation performance is the time taken for the algorithms to be executed. For the above simulations, 1000 particles were chosen as a higher number provided little improvement in attitude estimation accuracy, for a much higher computation cost. Since the computational time is highly reliant on the number of particles in the PF, the PF algorithm is run with a different number of particles '*N*', as shown in Figure 4, where the attitude estimation performance in terms of attitude RMSE is given. Table 3 provides the computational burden for each attitude estimation scenario relative to the EKF. PF-2 includes an extra step to calculate the quaternion from two sets of measurement vectors and therefore, has a generally higher computation time than PF-1. The inclusion of a sun sensor improves attitude estimation of a PF, but the computational time of PF-2 is higher than that of PF-1. Normally, a trade-off between computation time and attitude estimation accuracy is done to decide which performance metric is more appropriate for the attitude determination requirements of the small satellite mission. Comparatively, the EKF takes less time, albeit with sub-standard attitude estimation performance. While CubeSats are known for their limited computational and power resources, advances in the processors of onboard computers in small satellites may allow algorithms such as PFs to be used to achieve higher accuracies in attitude estimation for missions and payloads requiring higher accuracies of attitude pointing knowledge.

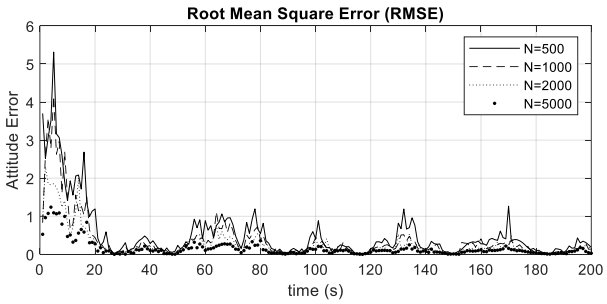

Figure 4: Plots of RMSE of attitude estimates for varied number of particles in PF.

Table 3: Computation burden comparison.

Attitude Estimation Algorithm	Computation Burden
EKF	1.00
PF-1 (N=500)	14.57
PF-2 (N=500)	15.17
PF-1 (N=1000)	21.62
PF-2 (N=1000)	24.31
PF-1 (N=2000)	40.61
PF-2 (N=2000)	45.28
PF-1 (N=5000)	93.13
PF-2 (N=5000)	89.19

CONCLUSION

Small satellite attitude and angular rate estimation via the particle filter algorithm are successfully achieved,

with two different attitude sensor configurations simulated. The estimation performances are compared with that of the EKF. The standard formulation of PF is used, and estimation performance compared when the weight update step in the PF algorithm is modified by using different sets of attitude sensor measurements. Simulation results confirm that the PF has superior attitude estimation accuracy, compared to EKF, having successfully achieved $\pm$ 0.01° pointing knowledge accuracy for attitude estimation and up to $\pm$ 0.006°/s for angular rate estimation. This is suitable for stringent attitude determination requirement in CubeSat missions. The attitude estimation performance of PF with two sensors, namely three-axis magnetometer, and sun sensor, was superior for attitude estimation, compared to PF-1, where only three-axis magnetometer was used. Besides the improvements in attitude estimation, this study shows that PF-1 and PF-2 exhibit quite similar angular rate estimation performance. The addition of sun sensors improved attitude estimation performance marginally, while also increasing computational time, as both sensor vector measurements needed to be fused before using the combined measurement to update the state and weights in PF-2. Generally, time, storage, and resources needed to execute the algorithm are all considered to decide whether a higher computation time is permitted. Future work will compare the implemented PF algorithm estimation results to other nonlinear attitude estimation schemes such as the UKF. The study offers a comparison for attitude estimation via PF in small satellite application where two different sets of attitude measurements are available. In a similar manner, other sensor combinations may be studied for feasibility of using PF in satellite attitude estimation.

REFERENCES

1. J. R. Raol, *Multi-Sensor Data Fusion with Matlab*. CRC Press, 2010.

2. Y. Cheng and J. Crassidis, "Particle Filtering for Sequential Spacecraft Attitude Estimation," *AIAA Guid. Navig. Control Conf. Exhib.*, 2004.

3. A. Carmi and Y. Oshman, "Adaptive particle filtering for spacecraft attitude estimation from vector observations," *J. Guid. Control. Dyn.*, vol. 32, no. 1, pp. 232–241, 2009.

4. S. Theil, P. Appel, and A. Schleicher, "Low Cost , Good Accuracy - Attitude Determination Using Magnetometer and Simple Sun Sensor," *Annu. AIAA/USU Conf. Small Satell.*, vol. 17, 2003.

5. S. Esteban, J. M. Girón-Sierra, Ó. R. Polo, and M. Angulo, "Signal conditioning for the kalman filter: Application to satellite attitude estimation with magnetometer and sun sensors," *Sensors (Switzerland)*, vol. 16, no. 11, 2016.

6. Y. Mimasu, J. C. Van Der Ha, and T. Narumi, "Attitude determination by magnetometer and gyros during eclipse," *AIAA/AAS Astrodyn. Spec. Conf. Exhib.*, no. August 2008, 2008.

7. Y. Liu, X. Jiang, and G. Ma, "Marginalized particle filter for spacecraft attitude estimation from vector measurements," *J. Control Theory Appl.*, vol. 5, no. 1, pp. 60–66, 2007.

8. R. A. J. Chagas and J. Waldmann, "Rao-Blackwellized particle filter with vector observations for satellite three-axis attitude estimation and control in a simulated testbed," *Rev. Control. Automação*, vol. 23, no. 3, pp. 277–293, 2012.

9. X. Jiang and G. Ma, "Spacecraft attitude estimation from vector measurements using particle filter," in *Proceedings of the Fourth International Conference on Machine Learning and Cybernetics, Guangzhou, 18-21 August 2005*, 2005, no. August, pp. 18–21.

10. Y. Yang and J. Li, "Particle filtering for gyroless attitude/angular rate estimation algorithm," *Proc. - 2010 1st Int. Conf. Pervasive Comput. Signal Process. Appl. PCSPA 2010*, pp. 1188–1191, 2010.